
Article:
Zhou, L. orcid.org/0000-0001-7760-832X, Zhang, J. orcid.org/0000-0002-3354-0690, Zhang, J. orcid.org/0000-0003-3750-6841 et al. (2 more authors) (2025) AMPLE: An adaptive multiple path loss exponent radio propagation model considering environmental factors. IEEE Transactions on Vehicular Technology, 74 (2). pp. 3395-3400. ISSN: 0018-9545

https://doi.org/10.1109/tvt.2024.3471655

AMPLE: An Adaptive Multiple Path Loss Exponent Radio Propagation Model Considering Environmental Factors

Lingyou Zhou, *Graduate Student Member, IEEE,* Jie Zhang, *Senior Member, IEEE,* Jiliang Zhang, *Senior Member, IEEE,* Oktay Cetinkaya, *Senior Member, IEEE,* and Stephen A. Jubb, *Member, IEEE*

***Abstract*—We present AMPLE — a novel multiple path loss exponent (PLE) radio propagation model that can adapt to different environmental factors. In the proposed model, the scenario under consideration is classified into region types from a raster map, and each type of region is assigned with a PLE. The path loss is then computed based on a straight line between the transmitter (Tx) and receiver (Rx), which records the intersected regions and the weighted region path loss. To regress the model, those PLEs are extracted via measurement and the region map. We also verify the model in two suburban areas and compare with the 3GPP path loss model and the Alpha-Beta-Gamma (ABG) model. The results show that the AMPLE model outperforms the aforementioned models. To the best of our knowledge, this is the first time that a practical multi-slope model precisely maps PLEs and region types. Besides, this model can be integrated into map systems by creating a new path loss attribute for digital maps.**

***Index Terms*—Path loss, prediction, radio propagation.**

I. Introduction

FOR channel modeling in the fifth generation (5G) or beyond 5G (B5G), it requires higher accuracy with much more complex propagation scenarios [1]–[3]. As one of the key parameters in large-scale parameters (LSPs), path loss predictions under 5G/B5G need to be simple and general, while possibly achieving higher accuracy. This is crucial as it further constrains the predictions of small-scale parameters (SSPs) in channel models [4]–[11]. That is, for the aim of enhancing channel model predictions, leaving LSPs such as path loss behind and focusing solely on the accuracy of SSP predictions would get only half the result with twice the effort.

Currently, deterministic and empirical models are the two most widely used categories of path loss models. Deterministic models, such as ray tracing and ray launching models [12], compute rays from Rx to Tx and from Tx to Rx based on ray optics, respectively. However, to maintain high prediction accuracy, these models require a large amount of computation resources and time. Empirical models, such as Okumura-Hata model [13], use a single characterization with a few parameters to calculate path loss for typical scenarios. Whereas, accuracy is sacrificed for maintaining minimum complexity and the type of scenarios is constrained to what the models are trained for. Also, in multi-slope models [14]–[17], while they segment propagation based on distance with different PLEs, break points, and additional losses for continuity, a practical and precise mapping between PLEs and region types is lacking.

To accurately predict path loss with low computational complexity, the geometry-based stochastic models (GBSMs) covered the path loss predictions for different scenarios [3]–[11]. Those path loss models including the close-in free space reference distance model with frequency-dependent path loss exponent (CIF), the ABG path loss model [4], and the 3GPP path loss models (as the extension of ABG model) [5]. The parameters in these path loss models can be either extracted from measurement data, or supplied by ray-tracing simulation results. However, an adaptive multiple PLE radio propagation model, which can automatically adapt its model parameters to different environmental factors, does not exist.

In this paper, we present a fast Adaptive Multiple Path Loss Exponent (AMPLE) radio propagation model considering environmental factors [18]. We first extract environment data by classifying raster maps into multiple region types, and each region type is labeled with a PLE that can be further determined via measurement. For path loss, a straight line between the Tx and Rx is generated, which records all the intersected regions and the weighted region path loss. The total path loss is computed in decibels by accumulating the weighted path loss of all the intersected regions within the straight line. We also apply the AMPLE model in two suburban areas for parameter regression and model validation, and compare to the ABG model [4] and the 3GPP path loss model [5]. The results show that the AMPLE model outperforms these models. To the best of our knowledge, this is the first time that the PLEs precisely corresponds to different region types in a practical multi-slope model. The current AMPLE model is a prototype which only considers path loss prediction and static environments. Also, this simple-but-accurate model can be integrated into map systems by creating a new path loss attribute for digital maps.

The rest of the paper is organized as follows. Section II describes the details of the AMPLE model. Section III demonstrates the AMPLE model in two suburban areas. Section IV summarizes and analyzes the parameter results of the

This work is funded by Innovate UK Project Radio Signal as a micro-Service (RSaaS). *(Corresponding author: Jie Zhang.)*

Lingyou Zhou is with the Department of Electronic and Electrical Engineering, The University of Sheffield, S10 2TN Sheffield, U.K., and also with Ranplan Wireless Network Design Ltd., CB23 3UY Cambridge, U.K.

Jie Zhang is with Ranplan Wireless Network Design Ltd., CB23 3UY Cambridge, U.K., and also with the Department of Electronic and Electrical Engineering, University of Sheffield, S10 2TN Sheffield, U.K.

Jiliang Zhang is with College of Information Science and Engineering, Northeastern University, Shenyang 110819, China.

Oktay Cetinkaya is with the School of Engineering, Newcastle University, NE1 7RU Newcastle upon Tyne, U.K.

Steve Jubb is with the Department of Civil and Structural Engineering, University of Sheffield, S10 2TN Sheffield, U.K.

This is the author accepted manuscript of an article published in IEEE Transactions on Vehicular Technology. The final published version is available at https://doi.org/10.1109/TVT.2024.3471655.

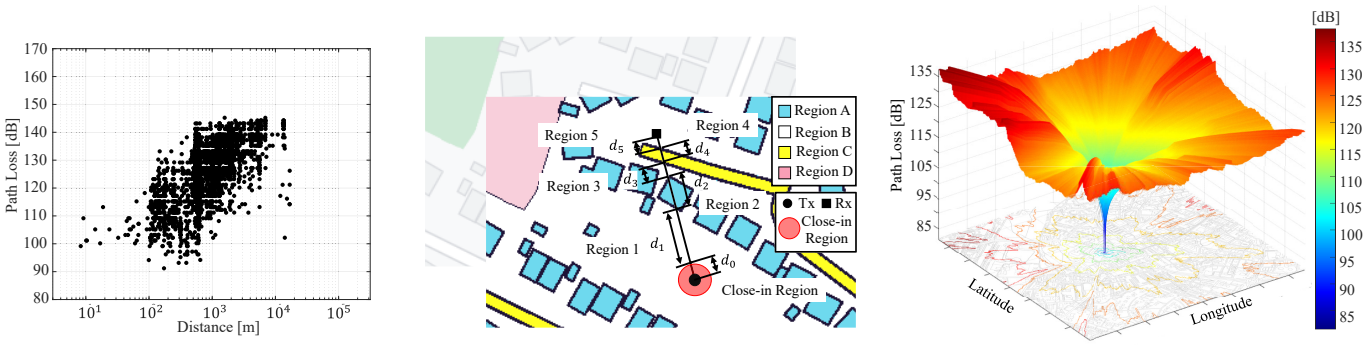

***Stage 1*: Measurement collection and analysis** | ***Stage 2*: Environment recognition and model construction** | ***Stage 3*: Parameter regression and path loss prediction**

Fig. 1. The process of constructing the AMPLE model.

AMPLE model in the measurement areas. Section V presents conclusions and future works.

II. The AMPLE Model

In this section, we first describe how to cover the environmental factors in the AMPLE model. We then present the construction details of the AMPLE model. Besides, we discuss the AMPLE model including its alternative constructing process and future prospects. A typical modeling process of the AMPLE model is shown in Fig. 1.

A. Map Classification with Straight Line

Based on the measurement of one Tx and multiple Rxs (an example is shown in the left side of Fig. 1), the path loss can be computed to serve as the foundation for model characterization. To incorporate environmental factors, a color-coded raster map of the measurement area is collected from map systems (e.g., Google Maps). By using k-means clustering based on the Euclidean distance of red, green and blue (RGB) values, environmental obstacles are classified into multiple region types. A straight line is then established for each Tx-Rx link, recording the intersected regions and the 2-dimensional (2D) region lengths, with an example shown in the middle of Fig. 1. It should be noted that the straight line is unrelated to line-of-sight (LOS) propagation in real-world scenarios, as LOS may not always occur in every link. The straight line can be expressed as

$$\mathbf{S} = \begin{bmatrix} R_0 & R_1 & R_2 & R_3 & \cdots & R_N \\ d_0 & d_1 & d_2 & d_3 & \cdots & d_N \end{bmatrix}, \quad (1)$$

where the first and second rows in (1) represent the intersected regions and the corresponding 2D region lengths. For common practice [13], [19], we set d_0 as the close-in distance, and the regions within d_0 are simplified as close-in region, which is illustrated in the middle of Fig. 1.

For real-world scenarios, the complex environments cause multiple propagation mechanisms, including reflection, diffraction, scattering, and penetration. Since different types of regions have its preference for different mechanisms (e.g., tree areas are more likely to have dense scattering, while street canyons may have the waveguide effect, resulting lower path loss), that is, parametrizing the region types will largely cover and reveal the whole propagation process without computing those mechanisms. So, even with a simple straight line, as we record and parametrize the intersected regions that carry the information of corresponding propagation mechanisms (i.e., directly influence path loss), the whole propagation can be modeled without compromising the fundamental principles of radio propagation [18].

B. The AMPLE Model

The decibel characterization of the AMPLE model for each Tx-Rx straight line can be expressed as

$$PL = C + \sum_{a=1}^{N} 10 n_a \log_{10}\left(\frac{\sum_{r=0}^{a} d_r}{\sum_{r=0}^{a-1} d_r}\right) + pX + \Psi_\sigma, \quad (2)$$

where C, N, n_a, d_r, X, p and Ψ_σ are characterized as follows.

- ***Intercept*** (C): For the straight line, C is the decibel path loss at close-in distance d_0 [13], [19]. Based on equation (2), regions within d_0 are not counted. Instead, d_0 is set as 1 m and the intercept C is regressed along with PLEs.
- ***Intersected Regions*** (N, n_a): There are N regions intersected by the Tx-Rx straight line, wherein n_a is the corresponding PLE for the ath region.
- ***Weighted Distance*** (d_r): d_r is the rth 2D region length, and the fraction in parentheses is the weighted distance to compute the weighted path loss for ath region. The numerator and denominator are summations ranging from close-in distance d_0 up to the lengths of ath and a-1th regions, respectively. By subtracting path loss between Tx to the ath region and Tx to the a-1th region in decibels, the weighted path loss of the ath region is computed.
- ***Penetration Loss*** (X, p): X is the penetration loss and p is the total number of penetrations in the straight line. Two penetrations (i.e., in & out) are considered when the straight line intersects buildings, while the model remains unchanged for the straight line passing through other region types (i.e., with corresponding PLE only). Note that we assume the penetrations will only occur for buildings (i.e., if the scenario does not contain such region type, p will be zero).
- ***Shadowing*** (Ψ_σ): The shadowing term Ψ_σ is normally distributed in dB-scale with $N[0, \sigma^2]$.

As the region types within the measurement area might not match the intersected regions N, equation (2) can be simplified by combining terms with the same PLE. That is, if there are M region types, the proposed model can be characterized as

$$PL = C + \sum_{m=1}^{M} D_m n_m + pX + \Psi_\sigma, \tag{3}$$

where n_m is the mth region type PLE, and D_m is the corresponding coefficient which is extracted by combining terms of n_m. Also, as the model in dB scale contains a shadowing term with normal distribution $N[0, \sigma^2]$, which means, the total path loss in this case is normally distributed with $N[\mu(C, n_m, X), \sigma^2]$, where [20]

$$\mu(C, n_m, X) = C + \sum_{m=1}^{M} D_m n_m + pX. \tag{4}$$

C. Discussion of the AMPLE Model

a) Relationship with the Log-Distance Model. From the above description, the AMPLE model is applicable to different scenarios according to different map-measurement sets. Thus, the quantity M may increase for complex scenario (e.g., multiple region types) and decrease for simple scenario (e.g., single region type). Specially, for scenario with single region type except building (i.e., $M = 1$ and $p = 0$), the (3) will be simplified to the log-distance model in decibels, which is [19]

$$PL = C + 10n \log_{10}(d/d_0) + \Psi_\sigma \qquad d \geq d_0, \tag{5}$$

with

$$\mu(d) = C + 10n \log_{10}(d/d_0), \tag{6}$$

where n is the PLE, C is the intercept that represents the path loss at close-in distance d_0, and (6) is the distance-dependent mean of normal distribution $N[\mu(d), \sigma^2]$ in dB-scale.

b) Distance or Weighted Distance? For traditional multi-slope models with multiple region types, path loss is computed directly based on distance, with additional losses added at break points between slopes to maintain model continuity [14]–[17]. However, for practical applications, especially in scenarios involving multiple region types, each transition between region types requires a distinct loss assignment (e.g., transitions between region types A, B, C, and D require six separate and unique losses). That is, as the complexity of environment increases, the number of losses for transitioning between region types grows, in addition to the PLEs for each region type. As a result, for such model type, the most commonly used model in practice is the dual-slope model only, which consists of a single break point dividing the model into two parts that roughly correspond to LOS and non-LOS (NLOS) scenarios.

Instead, by directly addressing the impact of region types to path loss (i.e., weighted path loss for intersected regions, calculated by weighted distance), there is no need to consider the discontinuity since the path loss is calculated by weight. So that, the model is largely simplified and can be deployed in multiple region types practically, along with the direct and precise relationship of "path loss — PLEs", instead of the indirect and rough "distance — PLEs" relations.

Also, from the weighted distance in the parenthesis of (2), the 2D distance can be potentially replaced by 3-dimensional (3D) distance (i.e., consider antenna height), as a simple ratio relation between hypothenuse and adjacent and the cancellation within that parenthesis based on trigonometric functions.

c) Alter Process of Constructing AMPLE. For the database, instead of measurement only, simulations made by ray-tracing can be alternatives. Besides, for map classification, only a basic machine learning method is used (i.e., k-means clustering), since the map data has been pre-processed (e.g., Google Maps). For general cases (e.g., raw map data like satellite maps) with arbitrary region shapes, deep-learning methods such as convolutional neural networks (CNNs) can be considered as alternatives.

d) Prospect of AMPLE. Although the propagation between Tx and Rx is depicted as a straight line shown in Fig. 1, all the radio propagation mechanisms are incorporated by different PLEs. Along with the model simplicity in (2) and (3), the AMPLE model achieves fast but accurate path loss prediction. Without changing construction, the AMPLE model can cover different scenarios according to different map-measurement (or map-simulation) sets, and it can be further added into the stochastic channel models (e.g., the 3GPP channel model [5]) for path loss prediction.

To the best of our knowledge, this is the first time that a practical multi-slope path loss model precisely maps PLEs to different region types. Beyond radio propagation, a new path loss attribute for digital map system is created by integrating the AMPLE model into map systems. Such integration generates part of a digital twin combining radio propagation loss and static environments. The developments in digital maps and machine learning have made the adoption of such a model feasible.

III. Model Application

In this section, we provide an application process of the AMPLE model in two suburban areas with measurements. We first present the data collection method within the measurement areas. Then, we describe the mapping between the region map and the data coordinates. In addition, the regression of model parameters based on the truncated data is given.

A. Measurement Collection

For the measurement data, we consider two scenarios for parameter regression and model validation, where they have the same propagation conditions. For parameter regression, the measured data are collected in Sheffield, U.K., considered as a suburban area with hilly terrain, dense buildings, and moderate-to-heavy tree densities [19]. We focus on a gateway of Long Range Wide Area Network (LoRaWAN) [21] that accommodates a LORIX One with a 4.15 dBi omnidirectional antenna. It is located on the Hicks Building (53.381029, -1.4864733) of the University of Sheffield, which has a height of 30 m. For the mobile antenna, Sheffield is mapped through "drive test" experiments, which are performed with autonomous mobile network scanner and field test device (having an antenna gain of 2 dBi), installed on an electric

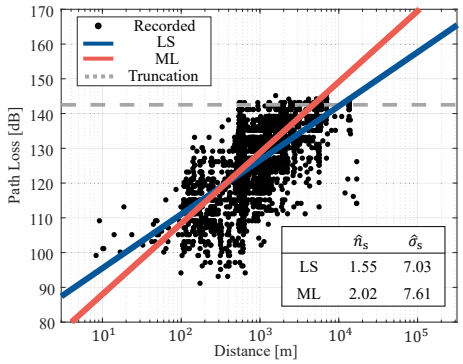

Fig. 2. The scatter plot of the measurement in Sheffield, and the estimation results of least-squares (LS) and maximum likelihood (ML) with truncated normal distribution.

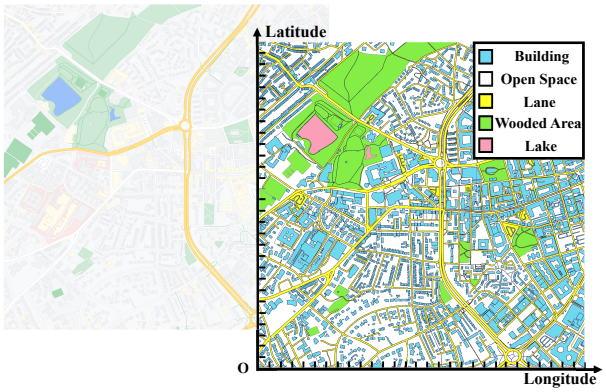

Fig. 3. Map classification in Sheffield, from the original raster map to the region map, along with the pixel coordinate system.

vehicle (an average height of 1.2 m). The received signal strength indicator (RSSI) are periodically recorded, together with the global positioning system (GPS) coordinates. Overall, the measurement data collected in Sheffield comprises 4615 data points transmitted around 868 MHz, with a transmitted power of 20 dBm. These data are taken at Tx-Rx separation distances ranging from several meters to 10 km. Since the antenna gains are included in RSSI [21], the path loss is calculated by subtracting the antenna gains of 6.15 dBi (4.15 dBi for Tx and 2 dBi for Rx) to exclude antenna effects.

Fig. 2 shows the scatter plot of 4615 measured path loss in meters. The gray dash line shows the truncation of measured data, while two straight lines represents two regression fit methods based on the log-distance model. Since the Rx detect limitation, path loss data beyond 142 dB is missing, leading to a bias in the estimated PLE and standard deviation of shadowing. This is evident in the blue line representing least squares (LS) in Fig. 2, resulting in $\hat{n_s} = 1.55$ and $\hat{\sigma_s} = 7.03$. To mitigate this, maximum likelihood (ML) with truncated normal distribution is employed [20], [22]. Based on equations (5) and (6), the probability density function (PDF) of zth measured path loss is given by [20], [22]

$$P(l_z;\mu(d),\sigma) = \begin{cases} \frac{1}{\sqrt{2\pi}\sigma} \frac{\exp\left(-\left(\frac{l_z-\mu(d)}{\sqrt{2}\sigma}\right)^2\right)}{\Phi\left(\frac{L-\mu(d)}{\sigma}\right)} & l_z < L, \\ 0 & \text{else}, \end{cases} \quad (7)$$

where L is the right truncated value as 140 dB, and Φ is the cumulative distribution function (CDF) of the standard normal distribution. By using (7) to regress the PLE and the standard deviation in the log-distance model, it yields more accurate results: $\hat{n_s} = 2.02$ and $\hat{\sigma_s} = 7.61$, as indicated by the red line in Fig. 2.

Meanwhile, for model validation, another set of measurement data is collected in Barnsley, U.K., which is considered a similar scenario to Sheffield (i.e., suburban area). The propagation conditions in Barnsley are also identical to those in Sheffield, including the transmission network, antenna type, collection method, and so on. The gateway in Barnsley is located on the roof of the Barnsley Digital Media Centre (53.5551977, -1.4789376), which has a height of 25 m. The measured path loss data in Barnsley consists of 631 data points, which also suffer truncation during data collection due to device sensitivity, and so that, the same truncation process is applied in this case. Similar to the measurements in Sheffield, the initial truncated PLE and standard deviation based on LS are $\hat{n_b} = 1.51$ and $\hat{\sigma_b} = 6.18$, respectively. After applying the truncation process (i.e., ML estimation with a truncated normal distribution [20], [22]), the PLE and standard deviation are $\hat{n_b} = 2.27$ and $\hat{\sigma_b} = 6.72$, respectively.

B. Region Classification and Coordinates Mapping

To extract the information of the environment, we collect raster maps of two scenarios from Google Maps, both with a map scale of 50 m and covering an area of approximately 2.25 km^2 (has a side of 2115 pixels). It should be noted that under the map constraints, 3128 out of 4615 measured path loss points are included in Sheffield, and 456 out of 631 measured path loss points are included in Barnsley. For region classification, we apply k-means clustering to identify regions with the same RGB values, and we combine the regions within the same type manually. While some errors occur during the clustering process, the overall classification results remain acceptable. Finally, the environmental obstacles in the two scenarios are classified into the following region types: *Building*, *Open Space*, *Lane*, *Wooded Area* and *Lake*. Taking Sheffield as an example, the original raster map and the classified region map are shown in Fig. 3.

Since the coordinates of Rx are recorded during experiments, the mapping between region map and measurement is to link the coordinates with region map. Based on the coordinates of map edges, the coordinate system is established and illustrated in Fig. 3, where each pixel can be constrained by its corner coordinates. For each Tx-Rx pair, the linear function of coordinates is generated to further record the intersected pixels. With exclusive-or algorithm, the intersected pixels can be finally constructed into the intersected regions.

C. Parameter Regression with Truncated Data

By setting region type M as five, we first calculate the PDF of (3) to process the truncation by ML with truncated normal distribution, which can be expressed as

$$P(l_z;\mu(C,n_m,X),\sigma) = \begin{cases} \frac{1}{\sqrt{2\pi}\sigma} \frac{\exp\left(-\left(\frac{l_z-\mu(C,n_m,X)}{\sqrt{2}\sigma}\right)^2\right)}{\Phi\left(\frac{L-\mu(C,n_m,X)}{\sigma}\right)} & l_z < L, \\ 0 & \text{else}, \end{cases} \quad (8)$$

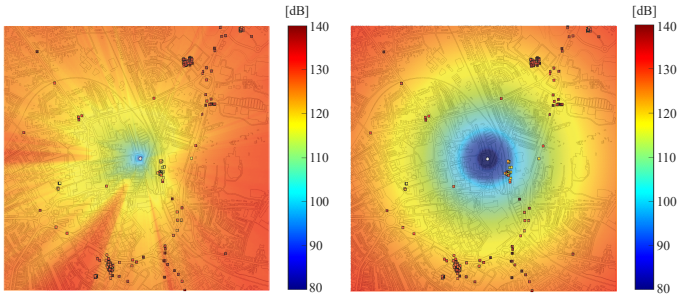

(a) (b)

Fig. 4. Heatmaps of the path loss prediction results predicted by (a) the AMPLE model and (b) the 3GPP-UMa model, in comparison with the measurements in Barnsley.

where $\mu(C, n_m, X)$ is expressed in (4), and other values in (8) are mentioned before. Based on (8), the likelihood function can be written as

$$F(\mu(C,n_m,X),\sigma)=\prod_{z=1}^{Z}\frac{1}{\sqrt{2\pi}\sigma}\frac{\exp\big(-\frac{(l_z-\mu(A,n_m,X))^2}{2\sigma^2}\big)}{\Phi\big(\frac{L-\mu(C,n_m,X)}{\sigma}\big)}. \tag{9}$$

To estimate the quantities of (8) by ML, the partial derivatives under natural logarithm of (9) for all the values are required, including PLEs n_m, intercept C, penetration loss X, and the standard deviation σ, which are

$$-\frac{\partial \ln F(n_m,C,X,\sigma)}{\partial n_m}=\sum_{z=1}^{Z}D_m\Bigg[\frac{\mu(C,n_m,X)-l_z}{\sigma^2}-\frac{\exp\big(-\big(\frac{L-\mu(C,n_m,X)}{\sqrt{2}\sigma}\big)^2\big)}{\sigma\int_{-\infty}^{\frac{L-\mu(C,n_m,X)}{\sigma}}\exp(-\frac{t^2}{2})dt}\Bigg], \tag{10}$$

$$-\frac{\partial \ln F(n_m,C,X,\sigma)}{\partial C}=\sum_{z=1}^{Z}\Bigg[\frac{\mu(C,n_m,X)-l_z}{\sigma^2}-\frac{\exp\big(-\big(\frac{L-\mu(C,n_m,X)}{\sqrt{2}\sigma}\big)^2\big)}{\sigma\int_{-\infty}^{\frac{L-\mu(C,n_m,X)}{\sigma}}\exp(-\frac{t^2}{2})dt}\Bigg], \tag{11}$$

$$-\frac{\partial \ln F(n_m,C,X,\sigma)}{\partial X}=\sum_{z=1}^{Z}p\Bigg[\frac{\mu(C,n_m,X)-l_z}{\sigma^2}-\frac{\exp\big(-\big(\frac{L-\mu(C,n_m,X)}{\sqrt{2}\sigma}\big)^2\big)}{\sigma\int_{-\infty}^{\frac{L-\mu(C,n_m,X)}{\sigma}}\exp(-\frac{t^2}{2})dt}\Bigg], \tag{12}$$

and

$$-\frac{\partial \ln F(n_m,C,X,\sigma)}{\partial \sigma}=\sum_{z=1}^{Z}\Bigg[\frac{1}{\sigma}-\frac{(\mu(C,n_m,X)-l_z)^2}{\sigma^3}-\frac{(L-\mu(C,n_m,X))\exp\big(-\big(\frac{L-\mu(C,n_m,X)}{\sqrt{2}\sigma}\big)^2\big)}{\sigma^2\int_{-\infty}^{\frac{L-\mu(C,n_m,X)}{\sigma}}\exp(-\frac{t^2}{2})dt}\Bigg], \tag{13}$$

where Z is the total data points (i.e., $Z = 3128$). Based on (10)-(13), the above parameters are combinatorially optimized by gradient descent with suitable step size.

IV. Results and Analysis

By setting d_0 to 1 m in (1) and applied the AMPLE model in Sheffield, the numerical values of PLEs are estimated combinatorically based on (8)-(13), and shown in Table I.

TABLE I
Model Parameters in the Measurement Area

Environmental Factors	Variables	Values
Intercept	C	81.54
In-Building	n_1	1.07
Open Space	n_2	1.71
Lane	n_3	2.45
Wooded Area	n_4	4.79
Lake	n_5	1.08
Penetration Loss	X	0.01
Standard Deviation	σ	6.97

Also, the physical analysis of these numerical values are given as follows.

- ***In-Building***: The predominance of teaching buildings and student accommodations in the measurement area, characterized by features like long corridors, induces an in-building waveguide effect. Moreover, since every building is divided into penetration and in-building cases, the blockage caused by this region type is represented by penetration loss X. These factors contribute to significantly lower in-building PLE compared to a measured case that is 1.57 [23].
- ***Open Space***: For the measured base station, it is located at the top of Hicks Building, which is situated at the hillside. Combined with the waveguide effect caused by other buildings, the n_2 is lower than 2.
- ***Lane***: For constantly moving vehicles (e.g., cars, buses and trams) on lanes which cause reflection, diffraction and scattering during the measurement [13], the value of n_3 is larger than 2.
- ***Wooded Area***: The intensive scattering caused by trees leads to severe loss, so the value of n_4 goes beyond 4.
- ***Lake***: When propagating through lakes at 868 MHz, the Sommerfeld-Zenneck surface waves are generated which is 10-20 dB stronger than space waves [24], [25]. That is, the signal decays as the quantity of n_5 because it propagates over the lake surface as a circle instead of radiating through the air as a sphere.

Based on PLEs in Table I which are regressed from measurements in Sheffield, we use the AMPLE model to predict the path loss of Barnsley and compare it to the 3GPP-UMa path loss model [5, Table 7.4.1-1]. Note that the base

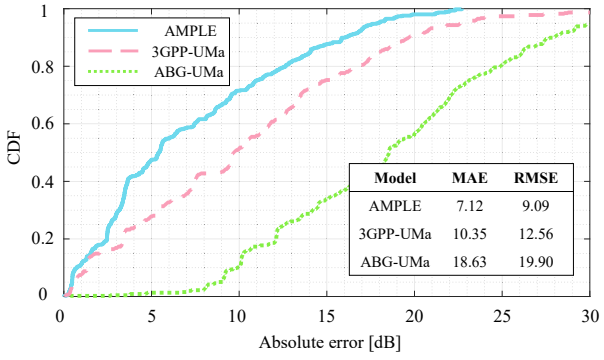

Fig. 5. CDF of absolute error between predictions (i.e., AMPLE, 3GPP-UMa, and ABG-UMa) and measurements in Barnsley.

station and user terminal antenna heights are set as 25 m and 1.5 m in 3GPP-UMa [5], respectively. In Fig. 4, we draw heatmaps of the two models and compare them with the measurement points in Barnsley, represented by squares with different colors indicating the level of path loss. Generally, by considering the environmental factors within the propagation scenario, the predictions of the AMPLE model are closer to the measurements, in comparison with the 3GPP-UMa model.

To provide a more intuitive comparison, we further deploy the ABG-UMa path loss model [4, Table 6] for the measurement area, and we draw the cumulative distribution functions (CDFs) to visualize the absolute error between these predictions and the measurements, as shown in Fig. 5. Besides, we compute the mean absolute error (MAE) and the root mean square error (RMSE) of those models in decibels (as shown in the bottom right corner of Fig. 5). Overall, the prediction of the AMPLE model outperforms the other models.

V. Conclusion and Future Works

We have presented the AMPLE path loss model with multiple PLEs considering environmental factors. We also applied the AMPLE model in two suburban areas and compare it with the 3GPP path loss model and the ABG model. The results show that the AMPLE model outperforms the 3GPP path loss model and the ABG model. The AMPLE model can not only be used to obtain fast and accurate path loss predictions, but can also be integrated into map systems by creating a new path loss attribute for digital maps. Therefore, the AMPLE model has the potential for wide applications and will have a significant impact in wireless communications.

For future works, the first is to deploy AMPLE into 3D case by considering antenna heights, and the impact of frequencies. Moreover, the AMPLE can be expanded to other large-scale parameters based on distance with log-normal distributions. Also, since the environmental factors are static in this prototype, it can be further expanded to cover dynamic environments such as moving vehicles. Finally, for raw map data with arbitrary region shapes, deep learning-based methods offer more precise map classification, yielding more detailed region types.

References

[1] J. Zhang *et al.*, "Channel measurement, modeling, and simulation for 6G: A survey and tutorial," 2023, arXiv: 2305.16616. [Online]. Available: https://arxiv.org/abs/2305.16616

[2] C.-X. Wang *et al.*, "6G wireless channel measurements and models: Trends and challenges," *IEEE Veh. Technol. Mag.*, vol. 15, no. 4, pp. 22–32, Dec. 2020.

[3] C.-X. Wang *et al.*, "A survey of 5G channel measurements and models," *IEEE Commun. Surv. Tutor.*, vol. 20, no. 4, pp. 3142-3168, 4th Quart., 2018.

[4] NTT Docomo, *5G channel model for bands up to 100 GHz, V2.0*, 2016. [Online]. Available: http://www.5gworkshops.com

[5] 3GPP, *Study on channel model for frequencies from 0.5 to 100 GHz, V16.1.0*, 2020. [Online]. Available: https://www.etsi.org

[6] S. Jaeckel *et al.*, *QuaDRiGa—Quasi deterministic radio channel generator, user manual and documentation, V2.0.0*, 2017. [Online]. Available: https://quadriga-channel-model.de

[7] V. Nurmela *et al.*, *METIS channel models, Deliverable D1.4,* 2015. [Online]. Available: https://www.researchgate.net/publication/282807948

[8] P. Kyösti *et al.*, *WINNER II Channel Models, D1.1.2 V1.0*, 2007. [Online]. Available: http://www.signal.uu.se/Publications/WINNER/WIN2D112.pdf

[9] M. Peter *et al.*, *Measurement campaigns and initial channel models for preferred suitable frequency ranges, Deliverable D2.1,* 2016. [Online]. Available: https://ec.europa.eu/research/participants/documents/downloadPublic?documentIds=080166e5a7a6b182&appId=PPGMS

[10] ITU-R SG05, *Draft new report ITU-R m. [IMT-2020.eval]*, 2017. [Online]. Available: https://www.itu.int/md/R15-SG05-C-0057/en

[11] L. Liu *et al.*, "The COST 2100 MIMO channel model," *IEEE Wireless Commun. Mag.*, vol. 19, no. 6, pp. 92–99, Dec. 2012.

[12] D. He *et al.*, "The design and applications of high-performance ray-tracing simulation platform for 5G and beyond wireless communications: A tutorial," *IEEE Commun. Surv. Tutor.*, vol. 21, no. 1, pp. 10–27, 1st Quart., 2019.

[13] T. S. Rappaport, *Wireless Communications: Principles and Practice*. New Jersey, USA: Prentice Hall, 1996.

[14] X. Zhang and J. G. Andrews, "Downlink cellular network analysis with multi-slope path loss models," *IEEE Trans. Commun.*, vol. 63, no. 5, pp. 1881–1894, Mar. 2015.

[15] J. Senic *et al.*, "Analysis of e-band path loss and propagation mechanisms in the indoor environment," *IEEE Trans. Antennas Propag.*, vol. 65, no. 12, pp. 6562-6573, Dec. 2017.

[16] P. Zhang *et al.*, "In-building coverage of millimeter-wave wireless networks from channel measurement and modeling perspectives," *Sci. China Inf. Sci.*, vol. 63, no.8, pp. 1-16, Aug. 2020.

[17] Y. Chang *et al.*, "A novel dual-slope mm-wave channel model based on 3D ray-tracing in urban environments," in *Proc. IEEE 25th Annu. Int. Symp. Pers. Indoor Mobile Radio Commun. (PIMRC)*, 2014, pp. 222-226.

[18] J. Zhang *et al.*, "A method of fast path loss calculation considering environmental factors," WO2023214176A1, 2023. [Online]. Available: https://patents.google.com/patent/WO2023214176A1/en?oq=WO2023214176A1

[19] V. Erceg *et al.*, "An empirically based path loss model for wireless channels in suburban environments," *IEEE J. Sel. Areas Commun.*, vol. 17, no. 7, pp. 1205–1211, July 1999.

[20] C. Gustafson *et al.*, "Statistical modeling and estimation of censored pathloss data," *IEEE Wireless Commun. Lett.*, vol. 4, no. 5, pp. 569–572, Oct. 2015.

[21] B. Eric, *LoRa documentation*, 2019. [Online]. Available: https://buildmedia.readthedocs.org/media/pdf/lora/latest/lora.pdf

[22] A. C. Cohen, *Truncated and Censored Samples: Theory and Applications.* New York, USA: Marcel Dekker, 1991.

[23] J. Miranda *et al.*, "Path loss exponent analysis in wireless sensor networks: Experimental evaluation," in *Proc. 11th IEEE International Conference on Industrial Informatics (INDIN)*, 2013, pp. 54-58.

[24] G. Peterson, "The application of electromagnetic surface waves to wireless energy transfer," in *Proc. IEEE Wireless Power Transfer Conference (WPTC)*, 2015, pp. 1-4.

[25] R. W. P. King, "Electromagnetic surface waves: New formulas and applications," *IEEE Trans. Antennas Propag.*, vol. 33, no. 11, pp. 1204–1212, Nov. 1985.